Topology and Toughening of Sparse Elastic Networks

Tetsuo Yamaguchi,[1] Yudai Onoue,[1] and Yoshinori Sawae[1,2]
[1]Department of Mechanical Engineering, Kyushu University, Fukuoka 819-0395, Japan
[2]International Institute for Carbon-Neutral Energy Research, Kyushu University, Fukuoka 819-0395, Japan

(Received 30 April 2019; revised manuscript received 5 December 2019; accepted 16 January 2020; published 12 February 2020)

The toughening of sparse elastic networks, such as hydrogels, foams, or meshes against fracture is one of the most important problems in materials science. However, the principles of toughening have not yet been established despite urgent engineering requirements and several efforts made by materials scientists. Here we address the above-mentioned problem by focusing on the topology of a network. We perform fracture experiments for two-dimensional periodic lattices fabricated from rubber strings and connecters with well-defined topological structures. We find that systematic increase in the largest coordination number while maintaining the average coordination number ($= 4$) as constant leads to significant improvement in toughness. We reproduce the observed toughening behavior through numerical simulations and confirm that the stress concentration in the vicinity of a crack tip can be controlled by the topology of the network. This provides a new strategy for creating tough sparse elastic networks, especially hydrogels.

DOI: 10.1103/PhysRevLett.124.068002

Sparse elastic networks are two- or three-dimensional structures composed of slender elastic bodies [1–8], such as chains, rods, or plates connected via nodes. Different examples with various mesh sizes can be found in numerous systems, such as low density amorphous ice [3], cytoskeletal networks [4], foams [5], knitted fabric [6], spider webs [7], and trusses [8].

Owing to their sparse structures, these networks provide important advantages, such as light weight, flexibility, permeability, and optical visibility [9]. However, there is a major drawback that must be overcome in many cases, i.e., brittleness under mechanical stresses. One typical example is hydrogels [10–18]. A hydrogel is a cross-linked polymer containing a large amount of water. This combination provides various kinds of unique properties and strong affinity to biological environments [13]. Despite these characteristics, the application of hydrogels to biomaterials has been extremely limited because of their brittle nature [14,15].

In the last two decades, novel types of hydrogels with improved toughness have been developed owing to the extensive efforts of materials scientists [10–12,16]. For example, double-network hydrogels [10] introduce structural heterogeneity in polymer networks, while slide-ring hydrogels [11] and tetra-polyethylene glycol hydrogels [12] are designed to reduce or relax stress concentration. These completely opposite strategies are known to contribute to toughening and motivate further developments [17–19]. However, the fundamental question of whether there is another novel method of toughening hydrogels remains to be answered.

The toughening of sparse elastic networks has been studied from other aspects in addition to hydrogels. The statistical properties of random elastic networks have been discussed by numerous researchers [20–22]. Recently, motivated by the study of the contact networks of granular systems [23], the effects of the average coordination number on the rigidity and failure of elastic heterogeneous networks have been discussed [24]. According to the results, as the average coordination number decreases and approaches a threshold ($= 4$), the width of the fracture process zone increases and the network toughens. This new kind of mechanical approach with a topological point of view [25–27] is currently expected as a promising strategy for developing novel mechanical properties and improving toughness. However, there are still only a few studies that have focused on the topology and fracture of periodic networks. These studies are considered to be important in designing and optimizing networks in a systematic manner.

In this Letter, we first investigate the effects of link length heterogeneity on toughness and then introduce a new aspect into sparse elastic networks, which is the topology of periodic lattices.

The schematic of the top view of our experimental system is depicted in Fig. 1(a). A sample of a sparse elastic network is pulled horizontally on a flat and slippery table by driving the top metallic bar at $V = 6$ mm/s until the sample breaks or the stroke reaches the maximum. The network is composed of links and nodes; a link, illustrated in Fig. 1(b), is fabricated from silicone rubber strings (diameter $D = 2$ mm, Young's modulus $E = 970$ KPa, RBWS2, Misumi), connecters, and cable clips. The network is assembled by coupling the connecters with bolts. To precisely control the force at break of each link, two cable clips are located at the center, where either of two rubber strings are pulled out at $F_{\mathrm{break}} = 5.5 \pm 0.1$ N. The

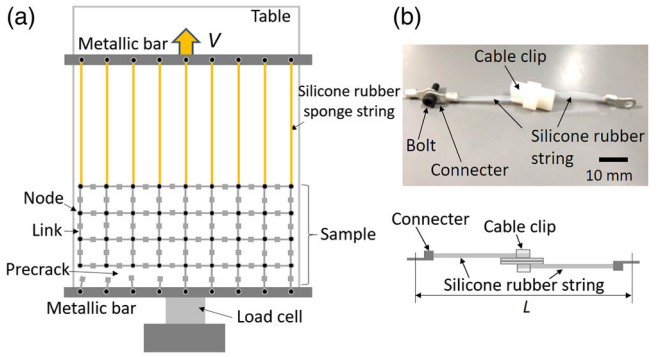

FIG. 1. (a) Top view of our experimental setup and (b) a link used in our sample.

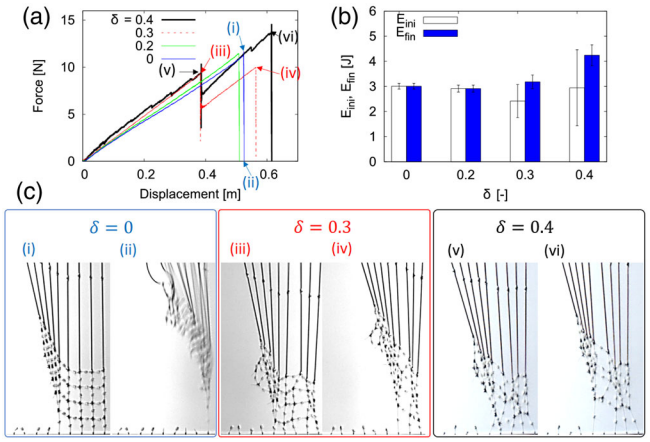

FIG. 2. Fracture behavior for samples with different degrees of link length heterogeneity δ. (a) Force-displacement curves, (b) fracture energies at initial break and final rupture, and (c) snapshots of the deformations, where numbers (i)–(vi) correspond to those shown in Fig. 2(a).

natural length and spring constant for the standard link are $L = 68$ mm ($L_R = 30$ mm for rigid parts and $L_S = 38$ mm for strings) and $k = 80$ N/m, respectively.

The sample is fixed with a metallic bar at the bottom end, and a precrack is introduced by disconnecting links over a certain length in advance. It is well known that the system with a crack becomes the most unstable in the stress-controlled loading condition [28]. However, this condition is not actually realized in the displacement-controlled testing machines. To test our samples under a severe condition, we intentionally reduce machine stiffness by connecting the softest (longest) possible strings (silicone rubber sponge strings, RBWSS3, Misumi, diameter $D = 3$ mm, length $L = 700$ mm, and spring constant $k = 7.1$ N/m) onto the sample at another end. Tensile displacement is represented by the stroke of the top metallic bar, and tensile force is measured using a load cell connected to the bottom bar at a sampling rate of 100 Hz. Fracture behavior is recorded by a CCD camera hung on the ceiling at 20 fps.

First, we study the effects of link length heterogeneity on toughness. Square lattice samples with different degrees of heterogeneity are prepared by randomly allocating short and long links, where one half of the links has length $L_{\text{short}} = L_0(1-\delta)$ and the other half has $L_{\text{long}} = L_0(1+\delta)$; thus, the link lengths are all different from $L_0 = 68$ mm but the average link length is L_0. The system size is $N_x = 9$ and $N_y = 5$ in the directions perpendicular and parallel to tensile force, respectively. Here, four different samples with $\delta = 0$, 0.2, 0.3, and 0.4, and with the same precrack length $N_{\text{crack}} = 4$, are examined. Figure 2(a) shows the force-displacement curves for the samples. It is clearly observed that all samples exhibit approximately the same elasticity at small strains (up to displacement $d = 0.35$ m) but show completely different behavior at large strains. For samples with $\delta = 0$ and 0.2, once a crack starts to propagate, it does not stop in the middle but ruptures the entire sample at around $d = 0.5$ m. In contrast, for samples with $\delta = 0.3$ and 0.4, a precursory break occurs at around $d = 0.4$ m, the samples continue to elongate, and complete rupture occurs at larger displacements ($d \sim 0.6$ m).

We define two types of fracture energies, E_{ini} and E_{fin}, to characterize fracture behavior. They are calculated by integrating the force-displacement curves until the initial break and final rupture, respectively. Figure 2(b) shows the fracture energies for four different samples, where the data for four trials are used to calculate the average values and the standard deviations for each type of sample. It is clearly seen that the variation in E_{ini} increases with δ. On the contrary, the variation in E_{fin} does not change significantly with δ and its average value increases for the samples with larger δ. This can be explained by the following mechanisms: while early break behavior is sensitive to the initial configuration of shorter or longer links and can fluctuate, the final rupture of the samples can be determined by the propagation of the main crack in "effective" media, where the early break of links efficiently dissipates stored elastic energy, works as sacrificial bonds, and contributes to delaying the propagation of the main crack [29,30]. Figure 2(c) shows the corresponding snapshots. Nonuniform link length distributions and highly heterogeneous rupture behavior are observed for the samples with large degrees of heterogeneity.

Next, we study the effects of network topology on toughness. We start from a regular square lattice as a trivial topological structure. From Maxwell's relation of structural rigidity, a square lattice without the bending stiffness of a link is known to exhibit anomalous behavior, such as vanishing shear elasticity at small strains [31]. Nevertheless, we adopt the square lattice as a benchmark because it is sufficiently simple, frequently seen as meshes or nets in daily life, and appropriate for observing the difference in topology and fracture behavior, as discussed later. Here, we create samples with different topological

structures by conserving the total number of nodes and links, where the average coordination number is the same for all samples. To simplify the discussion, we restrict ourselves to a periodic structure with a unit cell and locally change the coordination numbers within the cell. As a result, we systematically obtain a lattice with coordination numbers of 3 and 5 (named 3-5 lattice) and a lattice with coordination numbers of 2 and 6 (named 2-6 lattice), other than the square lattice. The system size is $N_x = 12$, $N_y = 7$, and $N_{\mathrm{crack}} = 4$. It is important to note that only one link exists at the crack tip to draw fair comparisons among different networks. However, differences exist in the total link length or weight; the total link length for the 3-5 and 2-6 lattices are 14% and 21% larger, respectively, than that of the square lattice. As is complemented in the Supplemental Material [32], they do not dominate the fracture behavior.

Figure 3(a) shows our experimental results. The samples with a larger difference in the local coordination number are more elongated, while the elasticity at small strains remains unchanged. Accordingly, as shown in Fig. 3(b), E_{fin} increases with the difference in the local coordination number. Surprisingly, E_{ini} also increases with the difference in the local coordination number. This suggests that the sparse elastic network can be toughened, not by introducing sacrificial bonds [29] or creating completely uniform [12] or relaxed structures [11], but by controlling the topology of the network.

We perform numerical simulations to investigate the mechanisms of the experimentally observed behavior. We model a node as a point mass m and a link as a linear spring with force at break F_{break}. The following equations of motion are numerically integrated with the forward difference method:

$$m\frac{d^2\vec{u}_i}{dt^2} = \sum_j \left[k_{ij}(l_{ij} - l_{0,ij})\frac{\vec{u}_j - \vec{u}_i}{l_{ij}} + \eta\left(\frac{d\vec{u}_j}{dt} - \frac{d\vec{u}_i}{dt}\right)\right], \tag{1}$$

where $\vec{u}_i$ is the position vector of the ith node, and $l_{ij} = |\vec{u}_j - \vec{u}_i|$ and $l_{0,ij}$ are the link lengths between nodes i and j with and without force, respectively. $k_{ij} = k_0 l_{\mathrm{ref}}/l_{0,ij}$ is the spring constant (k_0 being the constant for a reference natural length l_{ref}), and η is the viscosity for numerical damping. The sum is considered for all links connected to the ith node. In our simulations, we set $m = 1$, $l_{\mathrm{ref}} = 1$, and $l_0 = 1$ for the vertical and horizontal links and $= \sqrt{2}$ for the oblique links. In addition, $k_0 = 1$, $\eta = 0.2$, and $F_{\mathrm{break}} = 0.3$. We apply the force-free boundary condition on the left and right edges, and the zero displacement at the bottom end, except the precrack region (at N_{crack} points). Moreover, at each node at the top end, we apply linearly increasing tensile force $F_{\mathrm{ext}}(t) = \dot{F}t$ (where loading rate $\dot{F} = 2 \times 10^{-5}$) and zero displacement in the vertical and horizontal directions, respectively. As discussed in the Supplemental Material [32], the simulation condition is considered to be quasistatic except for larger square lattice samples with longer cracks [see also Fig. 5(a)].

Figure 4 shows the numerical results for the square and 2-6 lattices, where $N_x = 21$, $N_y = 11$, and $N_{\mathrm{crack}} = 5$. Note that there is only one link at the crack tip in both cases, similar to experiments. Figures 4(a) and 4(b) are the snapshots just before the initial break. It is clearly seen that the tensile force is highly localized in the square lattice, while it is widely distributed in the 2-6 lattice. Figures 4(c) and 4(d) show the normalized vertical forces of the bottom nodes $F_{y,y=0}/F_{\mathrm{break}}$, as a function of the horizontal distance

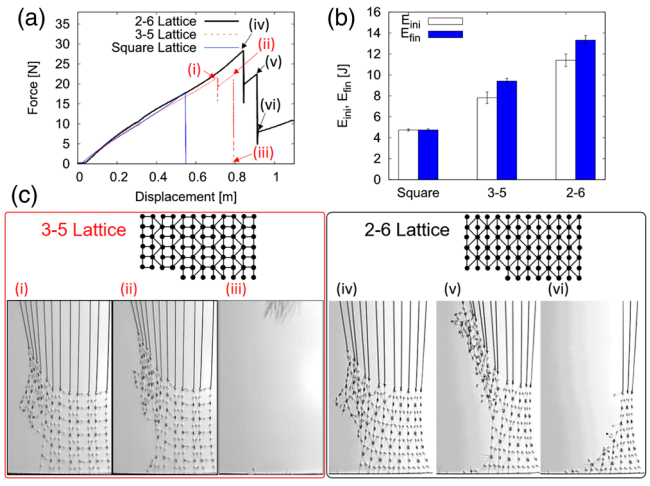

FIG. 3. Fracture behavior of samples with different topological structures. (a) Force-displacement curves, (b) fracture energies at initial and final rupture, and (c) snapshots of the deformations, where numbers (i)–(vi) correspond to those shown in Fig. 3(a).

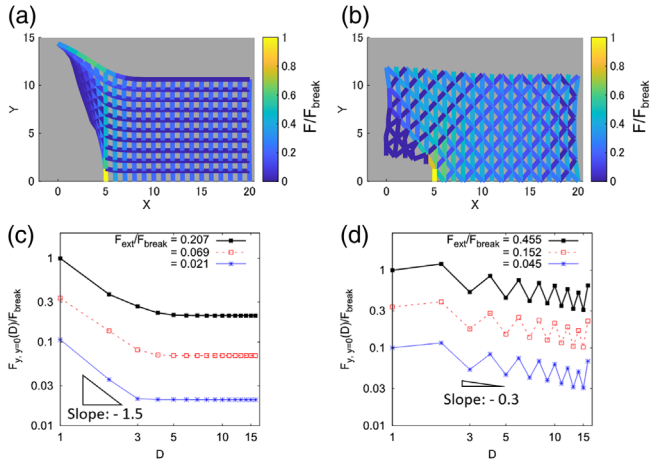

FIG. 4. Numerical results. Snapshots of the deformations just before the initial break for (a) square and (b) 2-6 lattices. Normalized vertical force distributions at three different external force levels as a function of the horizontal distance from the crack tip, obtained for (c) square and (d) 2-6 lattices.

from the crack tip $D(=X-N_{\mathrm{crack}}+1)$. The figures clearly show that, in the square lattice, the normalized force becomes the largest at the crack tip and decreases and approaches the external force level, $F_{\mathrm{ext}}/F_{\mathrm{break}}$, as D increases. The asymptotic behavior can be described by $F_{y,y=0}(D)/F_{\mathrm{break}} \sim D^{-1.5}$ for the three curves. In contrast, in the 2-6 lattice, the maximum force is not at the crack tip but at the next point. This is not surprising because there are one vertical and two oblique links connected to that node and the total forces supported by these links are calculated as tensile force. Furthermore, the overall trend (envelope) can be characterized by a power law with a significantly smaller exponent than that for the square lattice, $F_{y,y=0}(D)/F_{\mathrm{break}} \sim D^{-0.3}$, regardless of the external force level. The possible mechanism might be that nodes with larger coordination numbers create new "bypassing" routes, which essentially differs from that in double-network hydrogels [29] and in sacrificial bonds and hidden length [33]; it works even without a microscopic precursory break.

Finally, we discuss the relationship between precrack length N_{crack} and fracture strength $F_{\mathrm{ext}}/F_{\mathrm{break}}$, which is represented by the normalized external force at initial break. This corresponds to the inverse of the stress concentration coefficient [28]. We focus only on the initial break to discuss the effects of stress concentration. In these sets of simulations, four different system sizes are examined to study the finite size effects, i.e., $(N_x, N_y) = (81, 41), (61, 31), (41, 21)$, and (21,11). The numerical results obtained from different topological structures are shown in Fig. 5. In the case of the square lattice, all curves almost collapse into one curve, which is described as

$$F_{\mathrm{ext}}/F_{\mathrm{break}} \sim N_{\mathrm{crack}}^{-0.7} N_x^0. \tag{2}$$

This implies that fracture strength depends on crack length, but not on the system size. Note that fracture strength drops abruptly at $N_{\mathrm{crack}} \approx 20$ for larger samples ($N_x = 81$ and 61) due to shock fracture, which can be prevented by decreasing the loading rate.

On the contrary, in the 2-6 lattice, fracture strength depends on the system size and exhibits damped oscillatory behavior with the increase in N_{crack}. This oscillation can be simply understood; there is only one link attached when N_{crack} is odd (yielding smaller strength) and three links when N_{crack} is even (larger values). Then, we attempt to obtain master curves. For this purpose, we divide the data into two groups, odd and even, and then normalize the crack length based on system size N_x and strength based on $N_x^{-0.4}$. Our trial results are shown in Fig. 5(b). We can clearly see that the curves collapse into two curves for odd and even crack lengths, regardless of the system size. Based on this, we obtain scaling formulas

$$F_{\mathrm{ext}}/F_{\mathrm{break}} \sim N_x^{-0.4} f(N_{\mathrm{crack}}/N_x), \tag{3}$$

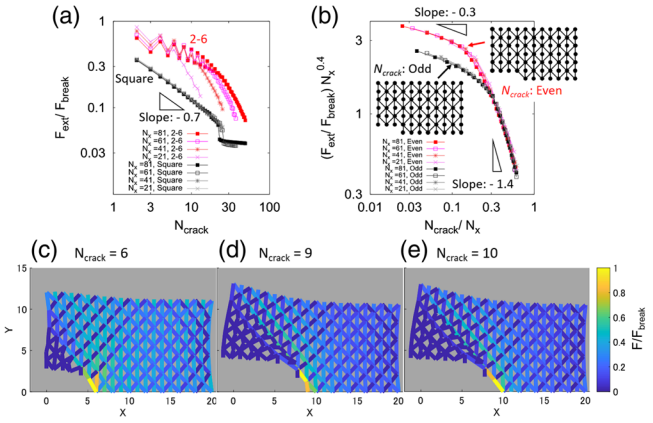

FIG. 5. (a) Crack length-normalized fracture strength curves for square and 2-6 lattices with various system sizes. (b) Master curves obtained for 2-6 lattices. Snapshots of the deformations for (c) $N_{\mathrm{crack}} = 6$, (d) 9, and (e) 10.

where $f(x)$ is a universal function that behaves irrespective of even or odd N_{crack} as $f(x) \sim x^{-0.3}$ for $x < x_c$ and $\sim x^{-1.4}$ for $x > x_c$. x_c ($\approx$0.3 and 0.2 for odd and even crack lengths, respectively) denotes the flexion point of the normalized curve. We compare the fracture strength between the square and 2-6 lattices by extrapolating the system size in the quasistatic loading limit [i.e., excluding the shock fracture shown in Fig. 5(a)]. As the ratio of strength between the two lattices becomes the largest at $N_{\mathrm{crack}}/N_x = x_c$, the maximum ratio can be calculated using Eqs. (2) and (3), $F_{\mathrm{ext,2-6}}/F_{\mathrm{ext,square}} \sim N_x^{0.3}$. This suggests that the 2-6 lattice becomes tougher than the square lattice as the system size increases.

In the final part of our discussion, we point out a few important features of the 2-6 lattice. First, fracture strength is larger for even N_{crack} compared to odd N_{crack} when N_{crack} is considerably smaller than N_x. This is because a larger number of links are connected to the bottom, as discussed previously and as evident from the comparison between the samples with $N_{\mathrm{crack}} = 5$ [Fig. 4(b)] and 6 [Fig. 5(c)]. Second, the strengths for $N_{\mathrm{crack}} = 9$ and 10 are almost the same. This can be understood by observing the snapshots; in the case of odd N_{crack} [Fig. 5(d)], the maximum elongation is not of the vertical link at the crack tip but the oblique link connected at the next node, which is similar to the case for even N_{crack} [Fig. 5(e)]. On the contrary, the mechanisms for the flexion of the curves are not so clear. Further investigation is required.

We studied the relationship between network structure and fracture behavior experimentally and numerically. We found that link length heterogeneity contributes to the introduction of sacrificial bonds in the sparse elastic network and delays the final rupture. We also found that the increase in coordination number difference decreases stress concentration and results in significant toughening. These results suggest a potential possibility of topological design

for tough elastic networks. However, further work remains to be done: for example, the optimization of the network structure, the combination of topology and link length variations, theoretical description, and extension to three-dimensional structures. These topics will be studied in the future.

T. Y. acknowledges A. Ikeda, H. Mizuno, T. Sano, H. Wada, B. Ravot, and J.-F. Molinari for their important suggestions. This work was supported by JSPS KAKENHI No. JP18H04486: "Discrete Geometric Analysis for Materials Design."

[1] B. Audoly and Y. Pomeau, *Elasticity and Geometry* (Oxford University, New York, 2010).
[2] T. G. Sano, T. Yamaguchi, and H. Wada, Phys. Rev. Lett. **118**, 178001 (2017).
[3] K. Koga, H. Tanaka, and X. C. Zeng, Nature (London) **408**, 564 (2000).
[4] D. Mizuno, C. Tardin, C. F. Schmidt, and F. C. MacKintosh, Science **315**, 370 (2007).
[5] I. Cantat, S. Cohen-Addad, F. Elias, F. Graner, R. Höhler, O. Pitois, F. Rouyer, and A. Saint-Jalmes, *Foams: Structure and Dynamics* (Oxford University, Oxford, 2013).
[6] S. Poincloux, M. Adda-Bedia, and F. Lechenault, Phys. Rev. X **8**, 021075 (2018).
[7] Y. Aoyanagi and K. Okumura, Phys. Rev. Lett. **104**, 038102 (2010).
[8] A. Carpinteri, *Structural Mechanics: A Unified Approach* (CRC Press, Boca Raton, FL, 2014).
[9] L. J. Gibson and M. F. Ashby, *Cellular Solids: Structure and Properties*, 2nd ed. (Cambridge University, Cambridge, England, 1997).
[10] J. P. Gong, Y. Katsuyama, T. Kurokawa, and Y. Osada, Adv. Mater. **15**, 1155 (2003).
[11] Y. Okumura and K. Ito, Adv. Mater. **13**, 485 (2001).
[12] T. Sakai, T. Matsunaga, Y. Yamamoto, C. Ito, R. Yoshida, S. Suzuki, N. Sasaki, M. Shibayama, and U.-I. Chung, Macromolecules **41**, 5379 (2008).
[13] J. Kopeček and J. Yang, Polym. Int. **56**, 1078 (2007).
[14] Y. Tanaka, R. Shimazaki, S. Yano, G. Yoshida, and T. Yamaguchi, Soft Matter **12**, 8135 (2016).
[15] T. Yamaguchi, R. Sato, and Y. Sawae, Gels **4**, 53 (2018).
[16] K. Haraguchi and T. Takehisa, Adv. Mater. **14**, 1120 (2002).
[17] J.-Y. Sun, X. Zhao, W. R. K. Illeperuma, O. Chaudhuri, K. H. Oh, D. J. Mooney, J. J. Vlassak, and Z. Suo, Nature (London) **489**, 133 (2012).
[18] F. Luo, T. L. Sun, T. Nakajima, T. Kurokawa, Y. Zhao, K. Sato, A. B. Ihsan, X. Li, H. Guo, and J. P. Gong, Adv. Mater. **27**, 2722 (2015).
[19] E. Ducrot, Y. Chen, M. Bulters, R. P. Sijbesma, and C. Creton, Science **344**, 186 (2014).
[20] H. J. Herrmann, A. Hansen, and S. Roux, Phys. Rev. B **39**, 637 (1989).
[21] P. Meakin, G. Li, L. M. Sander, E. Louis, and F. Guinea, J. Phys. A **22**, 1393 (1989).
[22] K. Kothari, Y. Hu, S. Gupta, and A. Elbanna, J. Appl. Mech. **85**, 031008 (2018).
[23] M. Wyart, L. E. Silbert, S. R. Nagel, and T. A. Witten, Phys. Rev. E **72**, 051306 (2005).
[24] M. M. Driscoll, B. G. Chen, T. H. Beuman, S. Ulrich, S. R. Nagel, and V. Vitelli, Proc. Natl. Acad. Sci. U.S.A. **113**, 10813 (2016).
[25] G. N. Greaves, A. L. Greer, R. S. Lakes, and T. Rouxel, Nat. Mater. **10**, 823 (2011).
[26] C. L. Kane and T. C. Lubensky, Nat. Phys. **10**, 39 (2014).
[27] S. D. Huber, Nat. Phys. **12**, 621 (2016).
[28] T. L. Anderson, *Fracture Mechanics: Fundamentals and Applications*, 4th ed. (CRC Press, Boca Raton, 2017).
[29] Q. M. Yu, Y. Tanaka, H. Furukawa,T. Kurokawa, and J. P. Gong, Macromolecules **42**, 3852 (2009).
[30] X. Feng, Z. Ma, J. V. MacArthur, C. J. Giuffre, A. F. Bastawros, and W. Hong, Soft Matter **12**, 8999 (2016).
[31] S. Alexander, Phys. Rep. **296**, 65 (1998).
[32] See Supplemental Material at http://link.aps.org/supplemental/10.1103/PhysRevLett.124.068002 for validation of simulation conditions and study of the effects of average link length on the fracture energy.
[33] B. L. Smith, T. E. Schäffer, M. Viani, J. B. Thompson, N. A. Frederick, J. Kindt, A. Belcher, G. D. Stucky, D. E. Morse, and P. K. Hansma, Nature (London) **399**, 761 (1999).